COVER PAGE

Bibliographical reference

A Study of Wideband Absorbers in a Non-Environment Control Room: Characterisation of the Sound Field by Means of p-p Probe Measurements, Soledad Torres-Guijarro, Antonio Pena, Alfonso Rodríguez-Molares and Norberto Degara-Quintela, Acta Acustica **vol. 97** (Number 1), 2011, pp. 82-92

DOI

https://doi.org/10.3813/AAA.918389

Acta Acustica united with Acustica
Vol. 97 (2011) 82 – 92

DOI 10.3813/AAA.918389

A Study of Wideband Absorbers in a Non-Environment Control Room: Characterisation of the Sound Field by Means of p-p Probe Measurements

Soledad Torres-Guijarro[1)], Antonio Pena[2)], Alfonso Rodríguez-Molares[2)], Norberto Degara-Quintela[2)]

[1)] Metrology Laboratory of Galicia (LOMG), Parque Tecnolóxico de Galicia, 32901 San Cibrao das Viñas, Ourense, Spain. storres@lomg.net

[2)] Sonitum, ETSI Telecomunicación, Universidade de Vigo, C/ Maxwell s/n, 36310 Vigo, Pontevedra, Spain. apena@gts.tsc.uvigo.es, amolares@gts.tsc.uvigo.es, ndegara@gts.tsc.uvigo.es

Summary

Wideband absorbers are a fundamental part of non-environment control rooms, providing high absorption in all the frequency range. They consist of huge angled panels hanging in front of the rear wall, the side walls, and the ceiling. As a first step to understand their absorption mechanisms, the sound field in the vicinity of the wideband absorbers of the rear wall has been measured with a p-p intensity probe in the control room at the 'Universidade de Vigo'. The characteristics of the sound field in the proximity of the rear wall will be discussed on the basis of the analysis of the pressure, particle velocity and intensity measurements.

PACS no. 43.20.Ks, 43.20.Mv, 43.20.Ye, 43.55.Ev, 43.58.Bh

1. Introduction

The non-environment room principle is a control room design concept that pursues the achievement of monitoring conditions as close as possible to free field conditions. These rooms can reduce the decay time of reflexions and modal energy to such low levels that the perception of many recording defects becomes much easier, and at the same time ensure compatibility amongst different control rooms built under the same principle, by virtue of their relative absence of monitoring acoustics [1].

In a non-environment control room, the side walls, the rear wall, and the ceiling are made as acoustically dead as possible to as low frequency as possible. The front wall is hard, dense and reflective, and the floor is also hard. These two surfaces provide acoustic life for sounds produced within the room, keeping comfortable working conditions. The loudspeakers are mounted flush in the solid front wall (see Figure 1), which provides a large baffle aiding the efficiency and uniformity of the low frequency radiation.

These rooms are made highly absorbent in all the frequency range thanks to the wideband absorbers that cover the side walls, the rear wall and the ceiling. The wideband absorbers are complex structures consisting of large panels that hang in front of a multi-layer absorbent surface. Although this absorbing structure has been successfully used for over 30 years, the fact is that only a few scientific studies have been done in order to demonstrate its behaviour. The most complete study was performed by Stuart Colam at the ISVR (Institute of Sound and Vibration Research, University of Southampton, UK). In his PhD thesis [2], Colam posed several hypotheses on the mechanisms of absorption of the wideband absorbers. After his work, three of these hypothesis hold for the absorption of the rear wall, which are summarised below.

1. Absorption due to ¼ wavelength resonances in the channels between panels. Adjacent panels and the multi-layer wall form closed end channels. At odd integer multiples of ¼ wavelength, the reflected sound from the wall will be in anti-phase with the incident sound at the opening of the channel. The acoustic impedance at this point and at these frequencies, will be purely real, and a maximum in the absorption will occur.
2. Attenuation of sound as it travels down the channels between panels, which effectively act as lined ducts. This effect is similar to the attenuation suffered by sound as it propagates along an air conditioning circuit lined with absorbent material. Below the cut-on frequency of the tube, where only plane waves can propagate, the attenuation of sound is poor, as the particle velocity normal to the duct boundary is not significant. The cut-on frequency equals the frequency of the first "transversal

Received 1 June 2010,
accepted 8 September 2010.

Figure 1. Non-environment control room.

mode" and is determined by the smallest transversal dimension of the channel.

3. Panels acting as waveguides, forcing the sound to be incident on the multilayer wall at a particular angle. The combined effect of panels plus multilayer wall is difficult to model, and would involve the study of the felt absorption under oblique incidence, which is probably larger than the normal absorption coefficient. Another related absorption mechanism is the "horn effect" which will be introduced in section 6.

As a first approach to verify these hypotheses, a detailed analysis of the sound field around the rear wall panels has been carried out based on in situ measurements in the control room at the 'Universidade de Vigo'. This control room was built by Philip Newell according to the non-environment principles, to be used as a high definition listening laboratory. Its acoustical behaviour has been analysed in [3, 4]. In these contributions it was shown that the combination of hanging panels and multilayer walls and ceiling behind them provides a high absorption coefficient (see Figure 11 for a typical absorption versus frequency curve of the rear wall), and therefore a good control of early reflections and decay tails, leading to a very short decay time, whose mean value is 165 ms.

Given the dimensions and construction characteristics of these absorbing structures, the analysis of their acoustic behaviour can only be carried out through in situ measurements. In this contribution, a p-p intensity probe has been used to perform the measurements. This common in situ measurement technique provides the waveforms of sound pressure from two coaxial, closely placed microphones. These waveforms are post-processed to compute the acoustic intensity and volume-velocity, and the analysis of these variables can shed light on the behaviour of the sound field. An exhaustive review of sound intensity measurement principles and applications and other related concepts can be found in [5].

This paper addresses the characterisation of the sound field in the vicinity of the wideband absorbers of the rear wall, as a first step to understand their absorption mechanisms. Its contents are organised as follows. Section 2 contains a detailed description of the wideband absorbers.

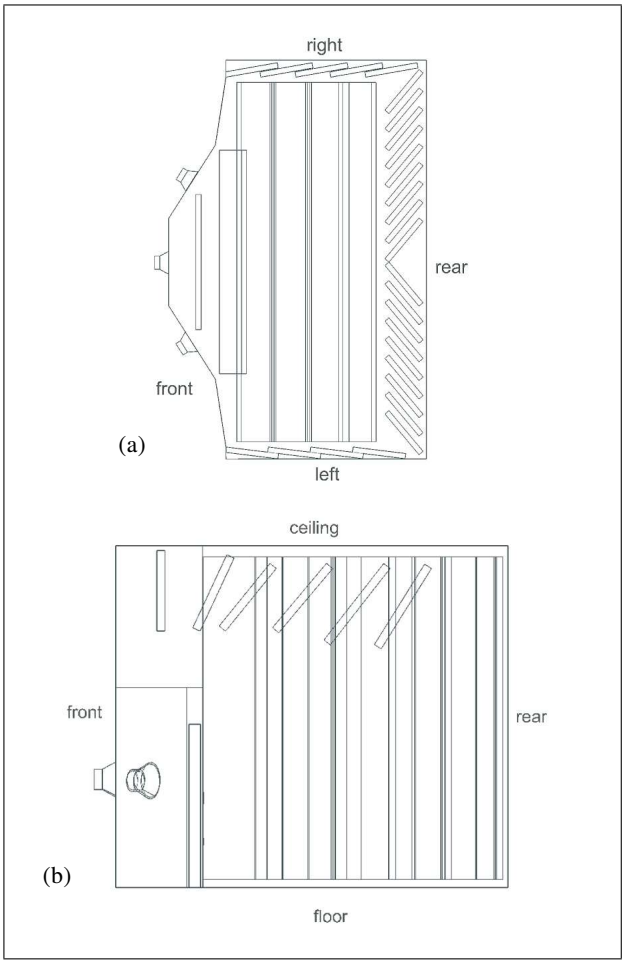

Figure 2. Panel placement inside the control room; (a) floor plan; (b) left elevation.

An initial picture of the sound field around the panels of the rear wall in this room has been obtained by FEM simulations, described in section 3. Following the traces of these simulations, and bearing in mind the previous studies [2], a set of measuring points was selected with the criterion of revealing the main characteristics of the sound field, as shown in section 4. The measured sound energy flux is shown by means of intensity maps, presented and discussed in Sections 5 and 6. The presence of standing waves and reactive fields is explored in Sections 7 and 8. Section 9 summarises the conclusions of this work.

2. Wideband absorbers

The wideband absorbers consist of large panels hung from chains in front of a multi-layer absorbent wall or ceiling. They fully cover the rear wall, the side walls, and the ceiling, as shown in Figure 2. Figure 3 shows a picture of the room under construction, before the rear and ceiling panels were covered with an acoustically transparent fabric.

The inclination of the panels in the rooms has been tested for years as numerous non-environment rooms were designed and built. The ceiling panels are inclined such that their leading edges point towards the loudspeakers,

Figure 3. Room under construction, rear and with ceiling panels uncovered.

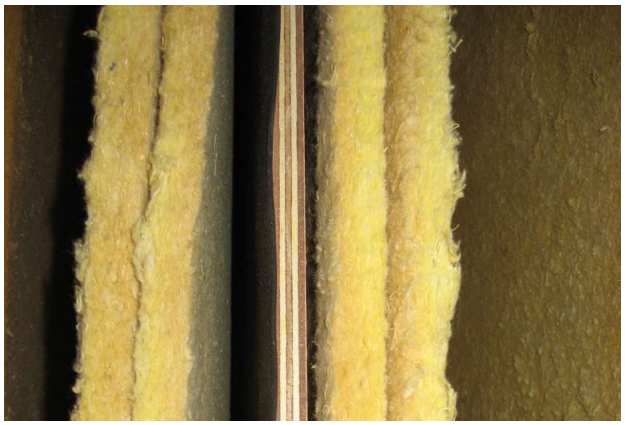

Figure 4. Panel construction.

Figure 5. Measured channel.

as shown in Figure 2, to provide the easiest access to the traps for the waves emitted by the loudspeakers. The lateral panels in this particular room hang at an approximate angle of 10° to the side wall. The rear panels, the object of this study, have an approximate angle of 40° to the rear wall. Their orientation is symmetrical with regard to the front-back axis of the room, and their dimensions are 1 m in width and over 4 m in height. They hang forming parallel channels with an approximate width of 12 cm between the outer cotton linings.

The construction of the panels can be seen in the picture in Figure 4: the core is a nominally 19 mm chipboard panel, but somewhat thinner plywood is also sometimes used, as in this case. Stapled to the board is a damping deadsheet of 3.5 kg/m^2. Both sides of the panels are covered in 4 cm thick, cotton-waste felt with a density of around 60 kg/m^3.

The walls and ceiling are constructed from a number of different layers [6], the innermost of them is cotton-waste felt. The panels and the wall are hidden behind an acoustically transparent fabric, which was partially removed for these measurements to give access to the channel where the intensity probe was located. Figure 5 shows the working area close to the rear wall.

3. FEM simulations

Some preliminary FEM simulations were performed to outline the behaviour of the sound field around the panels. A numerical model was posed consisting of a set of idealised panels disposed in a similar way to those in the rear wall. The idealised panels were composed of a 20 mm plywood core and a 50 mm cotton lining for each side. The damping deadsheet was not considered in the numerical model. The plywood core was simulated through an elastic domain of 615 kg/m^3 density and 12.4 GPa Young modulus. The porous domain was modelled through the Delany-Bazley model [7], which provides a characteristic impedance z_c and propagation constant k_c given by the empirical expressions

$$z_c = \rho_0 c \left[1 + 0.0571\left(\frac{\rho_0 f}{\sigma}\right)^{-0.754} - \mathrm{j}0.087\left(\frac{\rho_0 f}{\sigma}\right)^{-0.732}\right], \quad (1)$$

$$k_c = \frac{\omega}{c}\left[1 + 0.0978\left(\frac{\rho_0 f}{\sigma}\right)^{-0.7} - \mathrm{j}0.189\left(\frac{\rho_0 f}{\sigma}\right)^{-0.595}\right], \quad (2)$$

where ρ_0 is the density of air, c is the speed of sound, σ is the static flow resistivity, f is the frequency and ω is the circular frequency. The static flow resistivity of the porous domain has been chosen as 150 kNs/m^4, from the data available in the literature [8]. The elastic and the acoustic domains were directly coupled through a continuity condition on pressure and velocity.

Since the main interest was focused on the horizontal pattern of the sound field, not on its vertical variation, a 2D FEM model of the rear panels was constructed, in which the number, inclination, width, depth and distance between the panels, shown in Figure 6, were similar to the actual ones. In addition, for a better evaluation of the panels' performance, it was assumed that the back wall was totally

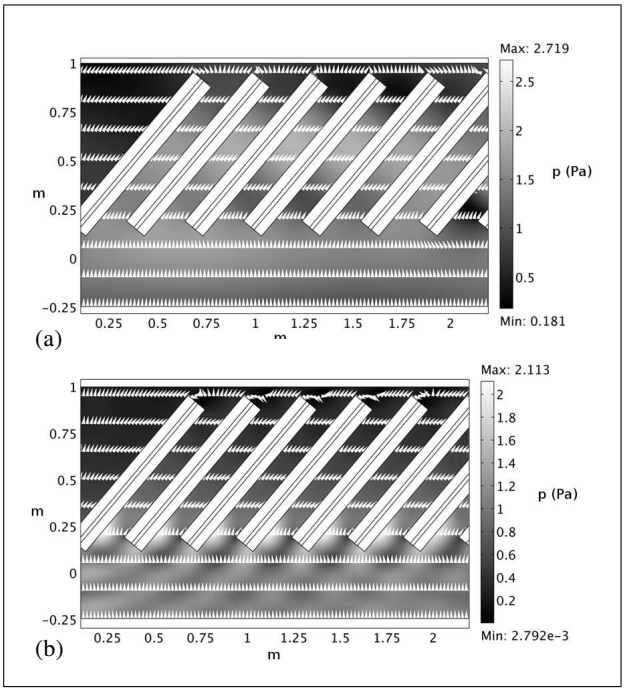

Figure 6. Numerical simulation results at (a) 200 Hz and (b) 1 kHz. Amplitude of sound pressure (in grey scale) and direction of the intensity vector (marked with cones).

absorbent. To achieve this, a 1-m thick perfectly matched layer [9] was set on the model rear boundary. The exciting signal was a pure tone progressive plane wave normal to the wall. The simulation was carried out at different frequencies from 200 Hz to 2 kHz. The sound source was simulated by setting a 5 m width harmonic Newman boundary condition on the front wall, located 2 m away from the panels, which makes it act as a perfectly rigid plane piston.

To guarantee a low numerical pollution, the quantity

$$\frac{kh}{2p} \tag{3}$$

in which k is the wave number, h is the maximum size of the elements and p is their order, has been kept less than 0.5 [10] in the entire frequency range. For both the acoustic and the elastic domains, the elements were chosen to be quadratic.

The results, shown in Figure 6, present the sound pressure and the sound intensity direction in the fluid domain. The white cones mark the sound intensity vector direction at each point of the fluid domain. Figure 6 clearly shows how panels "bend" the incident wave to change its direction to propagate along the channels, between them.

This guiding effect is clearly observed, in simulation, for frequencies up to 1.5 kHz. Theoretically, from 714 Hz, transversal modes start to propagate in the channel, provoking the sound energy to flow in different directions. However, the cotton linings seem to play a decisive role in spreading this wave guide behaviour at higher frequencies. The added absorption damps the transversal modes in the cavity, allowing only the longitudinal modes to propagate

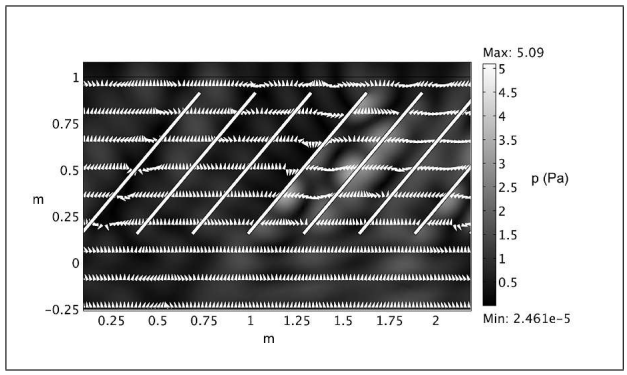

Figure 7. Numerical simulation results at 1 kHz when cotton linings are removed. Amplitude of sound pressure (in grey scale) and direction of the intensity vector (marked with cones).

in the channel. This effect is clearly showed in the simulation when the porous domains are removed. Figure 7 shows the sound field simulation at 1 kHz when the cotton linings were removed from the panels, and it can be compared to Figure 6b. As the white cones show, the direction of the intensity field is no longer parallel to the panels and the waveguide channel effect seems to disappear due to the propagation of the transversal mode in the channel.

The influence of the cotton lining can be demonstrated more instructively if it is shown as a function of the frequency. The angle of deviation θ of a sound intensity vector from the channel direction at any arbitrary point can be defined as

$$\theta = \arctan \frac{I_x}{I_y}, \tag{4}$$

where I_y is the intensity vector component in the channel direction and I_x is the intensity vector component in the normal direction. Figure 8 presents the evaluation of expression (4) in the point inside the channel (1.45, 0.55) for both situations, with and without the cotton linings. It is clearly seen that the wall lining improves the wave guiding effect up to 1.5 kHz.

To conclude, the effect of the panels is to change the direction of the incident wave so that it propagates along the channels. This guiding effect takes place in a similar way for all the channels, and for frequencies up to 1.5 kHz.

4. Measurement setup

One of the channels between the panels of the rear wall was selected for the measurements in the belief that its behaviour would closely resemble that of the rest of the channels of the same wall. The measured channel, shown in Figure 5, is located in front of the left loudspeaker (see Figure 2a), at roughly 1.8 m from the left wall and 5.2 m from the right wall.

The sound field has been studied through measurements at points 1 to 6 of Figure 9 (notice that the orientation of this figure is different to that of Figure 5: the upper part of Figure 9 corresponds to the rear wall). Points 1

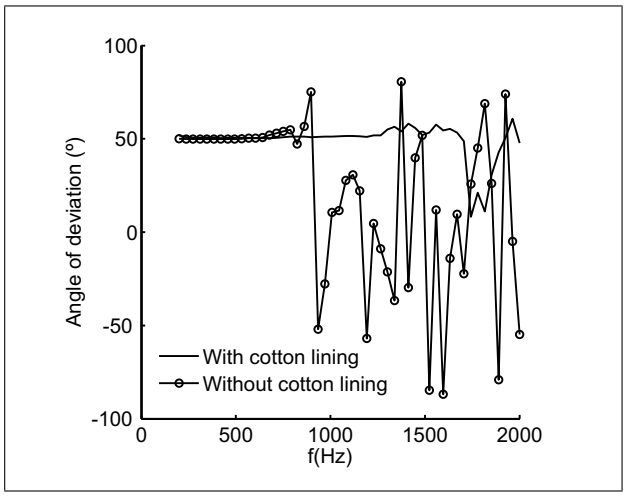

Figure 8. Angle of deviation of sound intensity vector from the channel direction at the point (1.45, 0.55) with and without the cotton linings.

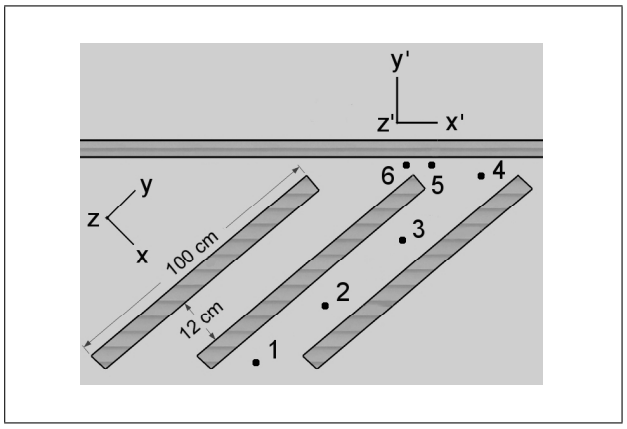

Figure 9. Measurement points in the channel between panels.

to 4 lie equally spaced in the middle of the channel, and were selected to analyse the sound guiding effect seen in the simulations. Points 5 and 6 are close to the gap between one of the panels and the rear wall, and were chosen to prove the existence of the so called "horn effect", discussed in section 6. All six points were measured at two different heights: height "a" (79 cm from the floor) and height "b" (30.5 cm from the floor). Henceforth, the measurement points will be identified as 1a,b to 6a,b.

The measurement instrument employed was a face-to-face p-p sound intensity probe (Brüel&Kjær 3595) whose pressure signals can be independently recorded through a PULSE front end. The probe was positioned at each measurement point in three orthogonal directions. The probe orientations are represented as rectangular coordinate systems in Figure 9. Note that two coordinate systems were used to facilitate the interpretation of the results: in the first system, denoted x-y-z, which was used for the measurements in the channel, the y axis is parallel to the panels; in the second system, denoted x'-y'-z', which was used for the measurements at points 5 and 6, the y' axis is perpendicular to the rear wall. The chosen microphone separation in the intensity probe was 5 cm, the largest available, to extend the lower measuring frequency limit as much as possible. In accordance with the data provided by the probe manufacturer, the available frequency range with this separation is 20 to 1250 Hz.

The stationary excitation signal used was pink noise radiated from the central loudspeaker of the control room, and the level was adjusted so that it generated a sound pressure level of 85 dBC measured at the sweet spot at the height of the monitors, which reasonably represents the normal working conditions of the room. Stationary tones of frequencies on the centres of the 1/3 octave bands were also employed. The reason for this excitation was to analyse the active/reactive intensity balance and assess the corresponding character of the sound field in different locations and frequencies.

The distance from the sound source to the closest measurement point is over 5 m. Taking $kr \gg 1$ as the condition to consider the wave reaching the probe as locally plane (k is the wavenumber and r the distance to the source), and considering that the product kr exceeds 10 for frequencies above 100 Hz and $r = 5$, it can be assumed that the waves that reach the panels are plane for all the simulated frequencies (200–2000 Hz) and almost all the measured range (20–1250 Hz), and that their direction of arrival is approximately normal to the rear wall.

The software associated with the probe (PULSE 7700), averages in time the sound intensity in the probe axis direction, providing the projection of the mean intensity vector in this direction in octave and one-third octave bands. In addition, the time-varying pressure signals were recorded and post-processed, in order to obtain the instantaneous and complex intensity estimations, and the pressure and particle velocity spectra.

In the following sections, these acoustic variables will be analysed to characterise the behaviour of the sound field in the proximity of the panels.

5. Waveguide effect

The waveguide effect outlined by the FEM simulations can be confirmed by the intensity maps inside the channel. Figure 10a shows, as an example, the intensity plot for points 1a to 6a in the 63 Hz octave band. Each vector in the plot represents the projection of the intensity vector in the horizontal plane, and is obtained by vector combination of the intensity measurements in the x/x' and y/y' directions. The excitation used was pink noise, and the intensity was computed in octave bands, to facilitate the comparison with the FEM results. It can be seen how the sound gradually changes its direction from normal incidence to the wall, to parallel to the panels. The vertical component (not shown here) is significantly smaller than the horizontal one. Similar results can be found in all the measurement range and at both heights, except for the 500 Hz band (see Figure 10b), which presents a somewhat irregular behaviour which will be analysed below.

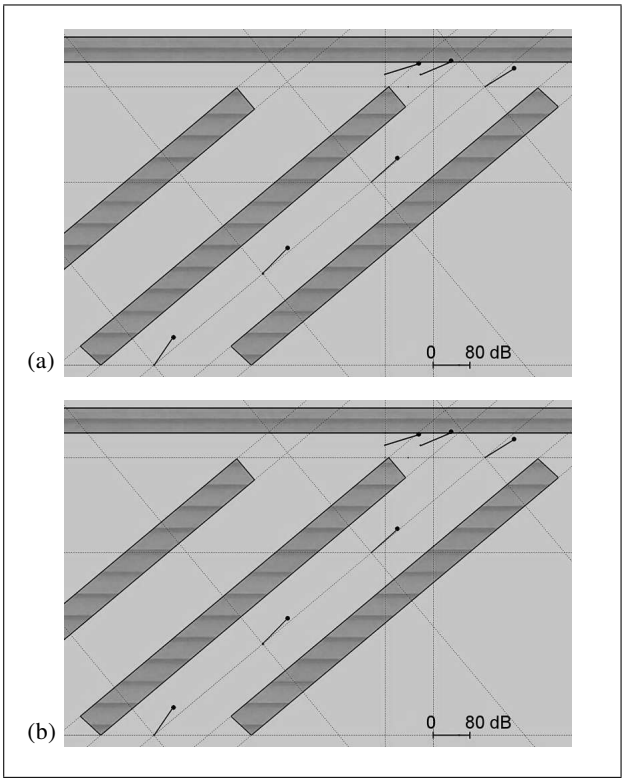

Figure 10. Intensity plot, horizontal plane, height "a", a) 63 Hz octave band, b) 500 Hz octave band.

The one-third octave measurements of the mean intensity confirm that the transversal component is small compared to the longitudinal one in most of the frequency range. This could be due to the waveguide effect, which produces a very small volume-velocity in the transverse direction, but it can also be argued that there might be hidden effects such as standing waves or reactive fields, that would not show up in a mean intensity representation. These kinds of sound fields will be analysed in sections 7 and 8.

6. "Horn effect"

The concept of the "horn effect" arose during the previously mentioned work of Stuart Colam at the ISVR [2]. This effect may constitute another mechanism which can explain the low frequency absorption at the panels. The underlying theory, outlined in [1] and detailed in [2], holds that the inclined panels would act like reversed horns, with the high particle velocity at the mouth of the channel giving rise to high pressure at the throat, where the panels almost touch the wall. The phase differences of the wavefront on each side of the panels, due to their waveguide effect, would lead to high particle velocities through the porous material covering the wall. In turn, this would give rise to considerable absorption due to resistive losses, at frequencies below the ones expected given the thickness of the porous material.

The existence of a "horn effect" in the area between the rear part of the panels and the back wall has been studied

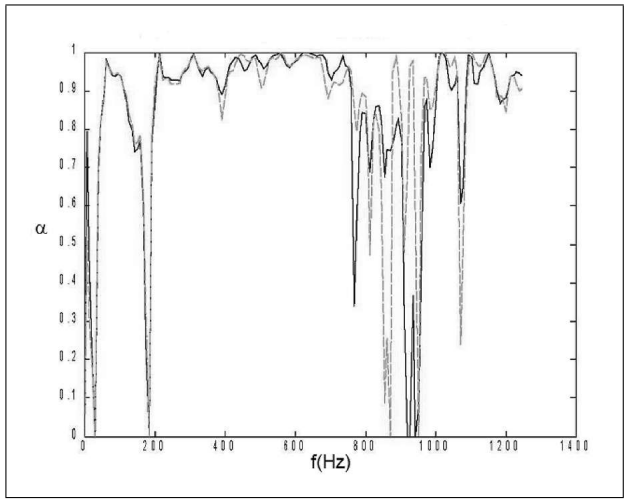

Figure 11. Normal absorption coefficient – – with and —— without gap filling.

through intensity, pressure and volume-velocity measurements at points 5 and 6. Intensity vector plots show a net energy flux from point 6 to point 5 at 63 Hz (both heights, see Figure 10a for an example) and 125 Hz (height "a"). Pressure results are very similar for all frequencies. The velocity component in the x' axis direction at those points is greater at some frequencies and smaller at others, compared to the y' components, but no consistent tendencies could be found. Thus, the only evidence of the existence of the horn effect seems to come from the intensity results at low frequencies.

In an attempt to maximise the impact of the "horn effect" on the absorption, the gap between the end of the panel and the wall was filled with cotton felt. Measurements at points 5 and 6 were repeated, and the results with and without the filling compared. No general tendencies, such as a clear decrease of the velocity in certain frequency range, could be appreciated. The absorption coefficient was also compared with and without gap filling, but again no significant differences could be found, as shown in Figure 11. This might be due to the fact that, if the "horn effect" contributes to the overall absorption, its contribution may be small, and hence may be masked by stronger effects. The procedure to compute the absorption coefficient and detailed absorption results will be presented in a subsequent contribution.

7. Transverse standing waves

The presence of a transverse standing wave is evident when the particle velocity in the three orthogonal directions is compared. Figure 12 shows the three components of the particle velocity measured in one-third octave bands at points 2a, 2b, 3a and 3b, as computed by PULSE. Points 2 and 3 were chosen for this study because they are situated close to the centre of the channel, where the guiding effect is well established, and the effect of the rear wall is weak.

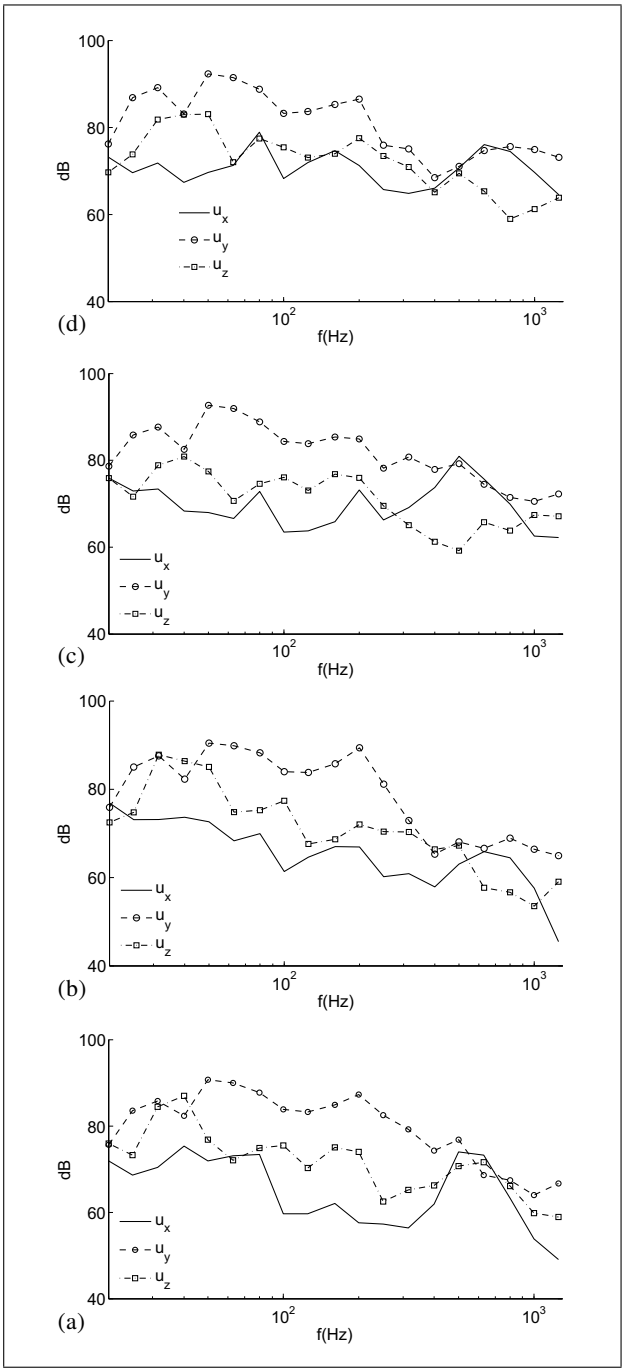

Figure 12. The three components of the particle velocity in third-octave bands: —— x, – – y, – · – z; (a) point 2a, (b) point 2b, (c) point 3a, (d) point 3b.

The y component, parallel to the panels, is clearly dominant in all the frequency range, except for an interval in the mid-frequency range where the x component has a noticeable rise, which can be related to the presence of a transversal standing wave. In the x component, a low Q resonance can be observed, which seems to correspond to a highly damped transversal standing wave formed between the panels. It should be noticed that the panels needed to be separated to make room for the probe, and are not strictly parallel. At height "a", the separation is 25.5 cm measured between plywood boards, thus the first transversal mode should appear at 680 Hz; at height "b" the separation is 31 cm, and the standing wave should be in 555 Hz. These results are in good agreement with the local maxima in the velocity spectra.

The high damping of the resonance may be due, at least partly, to the 4 cm thick cotton waste covering of the panels.

8. Reactive field

The presence of a reactive field is studied first through the pressure-intensity index computed for broadband excitation in third octave bands, as provided by the software of the probe. Then, the active/reactive intensity balance is analysed using steady-state tones as the excitation.

8.1. Pressure-intensity index

The pressure-intensity index, commonly denoted as δ_{pI}, is the most widely used sound field indicator, and is defined as the decibel difference between the measured levels of pressure and intensity. A plane wave propagating in free field in the probe axis direction would produce a very small value of the δ_{pI}. Several reasons can make δ_{pI} diverge from zero [5]: the probe axis is nearly perpendicular to the direction of the mean intensity; the field is partially reactive; the field is effectively diffuse; the field is produced by two or more sources which generate oppositely directed intensity vectors of similar magnitude at the measurement point; the intensity vector direction varies in such a way that the magnitude of the band integral vector is small in a frequency band.

In this case, given the probe orientation, the non-diffuse character of the sound field, the presence of a single source and the high measured mean intensity values, a high value of δ_{pI} can be expected to be given rise to the presence of a reactive field.

Intensity probe manufacturers provide maximum acceptable values of δ_{pI} for a given desired accuracy of the intensity measurement, which depends on the frequency range, the size of the spacer and the phase mismatch between the sensors.

Figure 13 shows δ_{pI} for the four points at height "a", in the three measuring directions. All the plots include as a reference the maximum value of δ_{pI} for our probe with the 5 cm spacer, when an accuracy better than ±0.5 dB is expected. The measurements at height "b" show a similar behaviour.

The analysis of the plots in Figure 13 reveals that δ_{pI} in the longitudinal (y) direction is smaller than the other two at almost all the points and frequencies. Furthermore, almost all the δ_{pI} values for the y axis are under the ±0.5 dB accuracy mask, which means that the sound field in this direction has a predominantly active character. This result confirms the conclusion derived from the mean intensity maps that the sound flows mainly in the longitudinal direction in the complete frequency range.

In the plots for the x and z axes, however, there are several points above the mask, most of them at low frequencies (below 200 Hz). The observation of the corresponding pressure and intensity levels (not shown here) reveals that those high values of δ_{pI} correspond to minimum mean intensity values, which may be related to the presence of a reactive field, as shown in the following analysis.

8.2. Active/reactive intensity balance

Up to now, the sound field around the panels has been mainly studied through the mean intensity, computed as the time average of the instantaneous intensity, defined as

$$\boldsymbol{I}(t) = p(t)\,\boldsymbol{u}(t), \tag{5}$$

where $\boldsymbol{I}(t)$ is the instantaneous intensity, $p(t)$ the sound pressure and $\boldsymbol{u}(t)$ the particle velocity. The bold notation is used to highlight the vector character of intensity and velocity. As the waveforms from the microphones in the probe, $p_1(t)$ and $p_2(t)$, were also recorded while performing the measurements, the time domain relationships between pressure and velocity, computed following the p-p principle of intensity measurement [5], can be analysed,

$$p(t) \approx \frac{1}{2}\left[p_1(t) + p_2(t)\right], \tag{6}$$

$$u_n(t) \approx \frac{1}{\rho_0 d}\int_{-\infty}^{t}\left[p_1(\tau) + p_2(\tau)\right]\mathrm{d}\tau, \tag{7}$$

where $u_n(t)$ is the particle velocity component in the direction of the probe axis, ρ_0 is the air density and d the gap between the microphones.

Once we have made this point clear, let us differentiate between three ideal, one-dimensional, stationary sound fields, described in terms of the phase relationship between the acoustic pressure and volume velocity:

Active field: the pressure and velocity are in phase (or anti-phase). The instantaneous intensity is always positive (or negative), and its value coincides with the mean intensity. This situation corresponds to a plane progressive wave producing a net energy flux in the direction of measurement.

Reactive field: the pressure and velocity are in quadrature, that is their phases are shifted 90 degrees. In this case, the instantaneous intensity oscillates around zero, its temporal average (mean intensity) is nil, and there is no net energy flux.

Standing wave: in this last case, the phase difference between pressure and velocity changes continuously. The energy flows alternatively in opposite directions, thus its mean value is again zero.

A real sound field is generally a mixture of these ideal situations, which can be modelled by splitting the instantaneous intensity into an active and a reactive component, associated with the components of particle velocity which are, respectively, in phase and in quadrature with the acoustic pressure.

The analysis of the relative phase between $p(t)$ and $\boldsymbol{u}(t)$, as a means of determining the active/reactive/resonant character of the sound field, can only be performed if the excitation is a single tone. When a more complex excitation is present, an equivalent insight can be obtained through the complex intensity. Among its possible definitions, the following has been chosen [11]:

$$I_c(t) = \frac{1}{2}\left[p(t) + \mathrm{j}\hat{p}(t)\right]\left[\boldsymbol{u}(t) - \mathrm{j}\hat{\boldsymbol{u}}(t)\right], \tag{8}$$

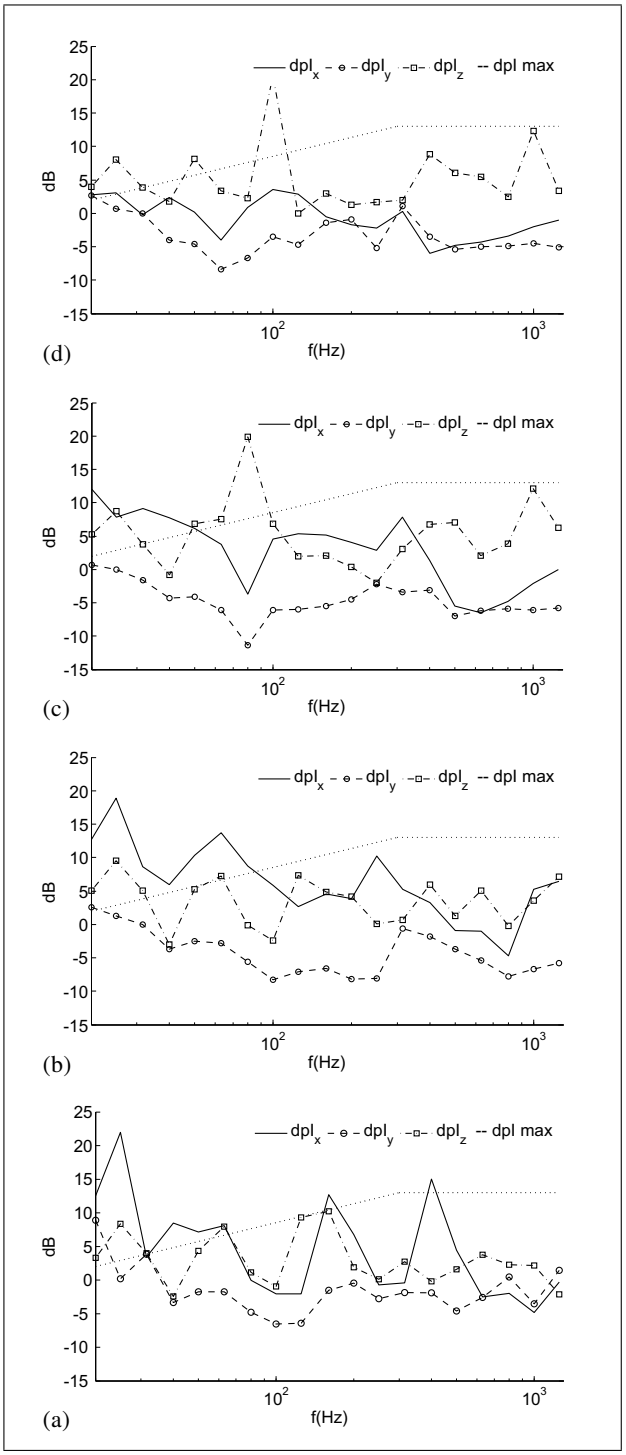

Figure 13. δ_{pI} in the three axes for points a) 1a, b) 2a, c) 3a, d) 4a.

where $\hat{p}(t)$ and $\hat{\boldsymbol{u}}(t)$ are the Hilbert transforms of $p(t)$ and $\boldsymbol{u}(t)$, respectively.

In a narrowband field, the real and imaginary parts of are low pass signals that represent the short-time temporal averages of the active and reactive instantaneous intensity components.

In the following, the transversal acoustic field with tonal excitation at some points and frequencies will be analysed by means of the pressure-velocity relative phase, the instantaneous intensity, and the real and imaginary parts of the complex intensity computed from (8), and the δ_{pI}. In analysing the following figures, it should be taken into account that the pressure and velocity waveforms have been independently scaled to plot them together (thus their amplitudes should be ignored), that the intensity is plot on linear scale, and that the δ_{pI} was obtained with broadband excitation.

Figure 14 shows the analysis at point $2b$, x axis (normal to the panels), when a pure tone of 400 Hz is used as excitation. The pressure and velocity waveforms are 90° out of phase, the instantaneous intensity oscillates around a value close to zero, the real part of the complex intensity is considerably greater than the imaginary part, and the δ_{pI} value corresponding to the third octave band centred in 400 Hz shows a peak above the ±0.5 dB accuracy mask. Thus, at this point, frequency and orientation, all the signs point to a strong reactive field.

Figure 15 shows the analysis at point 3a with a 315 Hz tone. In this case, the phase difference between pressure and velocity, the mean value of the instantaneous intensity, and the amplitudes of the real and imaginary components of the complex intensity point to a dominant reactive field. But the δ_{pI} is small, well below the mask, and does not even show a local maximum. This disagreement may be due to the fact that the value of δ_{pI} at 315 Hz is the result of frequency averaging across the corresponding third octave band. If the reactive field at this measuring point is dominant at 315 Hz, but is not so in the rest of the band, it will probably not show up in the δ_{pI} representation.

The two cases studied prove the existence of a reactive field inside the channel at certain frequencies. The first case (2b, 400 Hz) is the most conclusive, since there are high values of both δ_{pI} and reactive intensity. In the other case (3a, 315 Hz) there are also signs of the presence of a reactive field in the analysis through the tonal excitation.

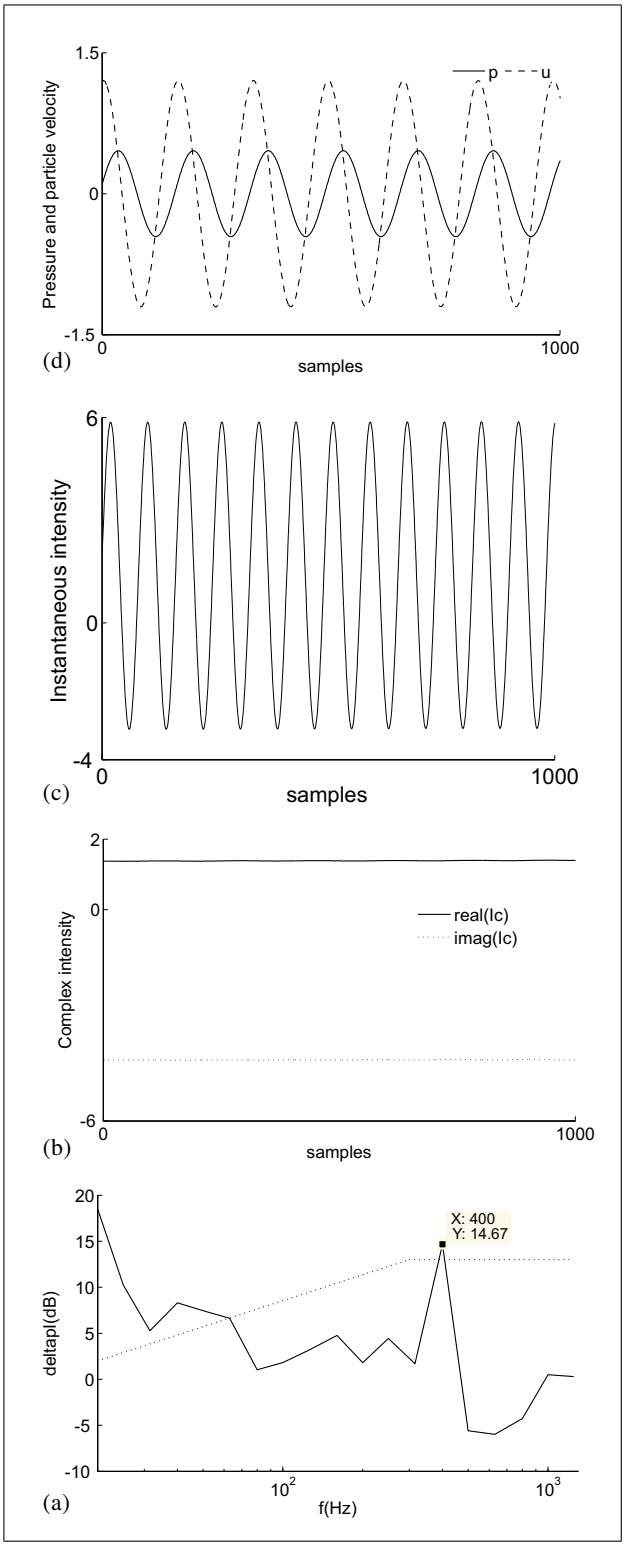

Figure 14. Active/reactive field analysis at point $2b$, x axis, 400 Hz: (a) pressure and particle velocity, (b) instantaneous intensity, (c) complex intensity, (d) δ_{pI}.

9. Conclusions

The aim of this work has been to characterise the sound field near the wideband absorbers of the rear wall of the control room at the 'Universidade de Vigo', as a first step to understanding their high absorbing properties at low frequencies. FEM simulations were performed first in order to outline the behaviour of the sound field and decide on the measuring points inside the channel between two panels. Then, a set of measurements with a p-p probe were performed in the 20–1250 Hz range, and several acoustic variables derived from the microphone signals were analysed.

The FEM simulations and the mean intensity maps show a clear waveguide effect: the sound that arrives at a normal angle to the rear wall changes its direction to

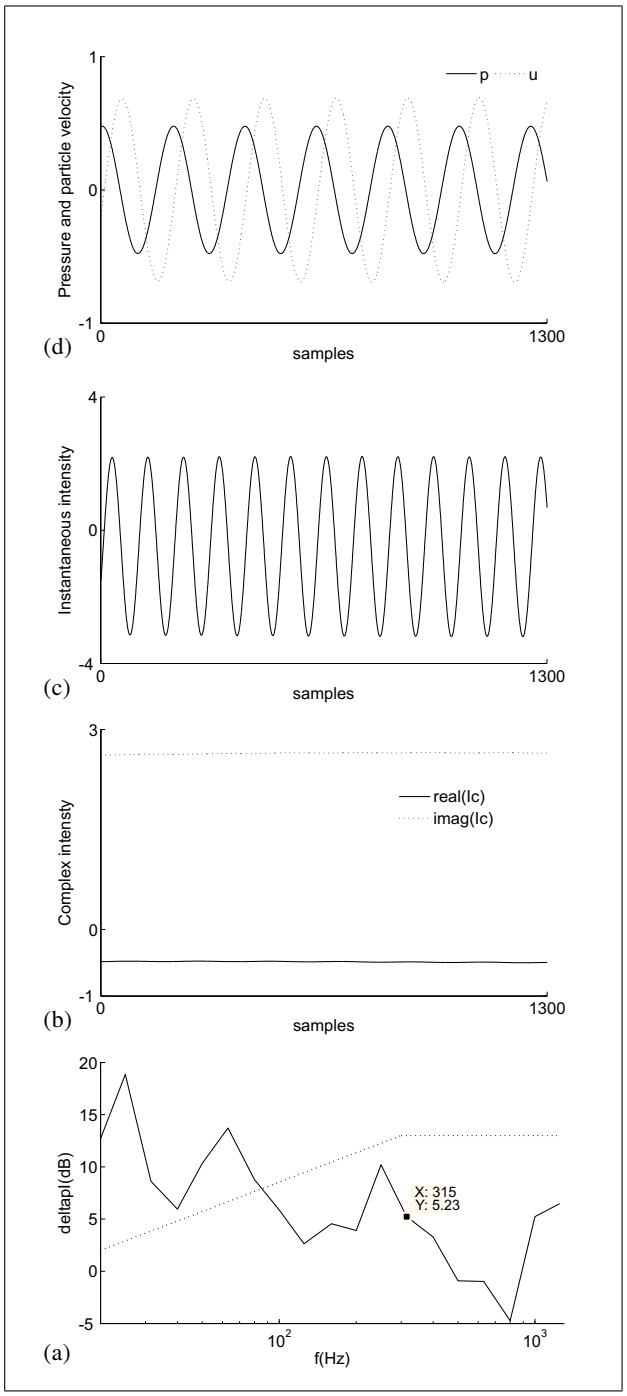

Figure 15. Active/reactive field analysis at point 3a, x axis, 315 Hz: (a) pressure and particle velocity, (b) instantaneous intensity, (c) complex intensity, (d) δ_{pI}.

propagate along the channels between the panels. The net energy flux is therefore parallel to the panels and towards the rear wall. The analysis of the particle velocity spectra confirms that the longitudinal component is predominant, except for a low Q transversal resonance, related to the first standing wave that develops between the panels.

The presence of a reactive field inside the channel has also been analysed. The third-octave band plots of δ_{pI} shows the predominance of an active sound field in the longitudinal direction, while higher values of δ_{pI} can be seen in the other two orthogonal directions at some frequencies, mostly below 200 Hz. Two case studies where explored through the analysis of the pressure-velocity relative phase, the instantaneous intensity and the complex intensity with tonal excitation. In one of them, these analyses pointed to the presence of a reactive field in agreement with a high δ_{pI} value, while in the other the results were not so conclusive.

To conclude, the main effect of the panels on the sound field generated in the front part of the room is to force the waves to propagate along the channel between them, with a net energy flow being evident in this direction. There is also a significant transversal velocity near the first standing wave frequency. The reactive field cannot be considered as dominant between the panels, and the significance of the horn effect has still not been proved. The relationship between these effects and the absorption measured in front of the panels will be established in a subsequent contribution.

Acknowledgement

The authors wish to thank Philip Newell, the designer of the control room under study, for his invaluable and continuous help with the research work undertaken in our group; Finn Jacobsen, for his helpful comments on the first draft of this paper; and Carmen Gómez Jorge and José M. Caurel Carrera, students at the 'Universidade de Vigo', who performed the measurements.

Role of the founding source

This work has been partially supported by the Spanish Department of Education and Science, under the project TEC2006-13883-C04-02 "Sound source separation for acoustic measurements, AnClaS3", and by the Galician Department of Economy and Industry through the Human Resources Programs "Isidro Parga Pondal" and "Isabel Barreto".

References

[1] P. Newell: Recording studio design. Focal Press, Oxford, 2003.

[2] S. Colam: An investigation into an empirically designed passive sound absorber for use in recording studio control room. PhD Thesis, ISVR, University of Southampton, 2002.

[3] S. Torres-Guijarro, A. Pena, N. Degara-Quintela: Objective evaluation of a non-environment control room for 5.1 surround listening. AES 124th Convention, Amsterdam, The Netherlands, May 17-20, 2008.

[4] S. Torres-Guijarro, A. Pena, M. A. Sobreira-Seoane: On the use of a non-environmental control room as a 5.1 surround listening room. Proc. 19th International Congress on Acoustics, Madrid, Spain, September 2-7, 2007.

[5] F. J. Fahy: Sound intensity, 2nd ed. E&FN Spon, London, 1995.

[6] S. Torres-Guijarro, A. Pena, A. Rodríguez-Molares, N. Degara-Quintela: Sound field characterisation and absorption measurement of wideband absorbers. AES 126th Convention, Munich, Germany, May 7-10, 2009.

[7] M. E. Delany, E. N. Bazley: Acoustical properties of fibrous absorbent materials. Appl. Acoust. **3** (1970) 105–116.

[8] L. L. Beranek, I. L. Ver: Noise and vibration control engineering and applications. John Wiley and Sons Inc., New York, 1992.

[9] J.-P. Bérenger: A perfectly matched layer for the absorption of electromagnetic waves. J. Comput. Phys. **114** (1994) 185–200.

[10] F. Ihlenburg: Finite element analysis of acoustic scattering. Appl. Math. Sci. **132** (1998) Springer–Verlag, New York.

[11] F. Jacobsen: A note on instantaneous and time-averaged active and reactive sound intensity. J. Sound Vib. **147** (1991) 489–496.